Three-dimensional mapping by CryoSat-2 of subglacial lake volume changes

Malcolm McMillan,[1] Hugh Corr,[2] Andrew Shepherd,[1] Andrew Ridout,[3] Seymour Laxon,[3] and Robert Cullen[4]

Received 13 May 2013; revised 20 June 2013; accepted 20 June 2013.

[1] We analyze data acquired by the CryoSat-2 interferometric radar altimeter and demonstrate its novel capability to track topographic features on the Antarctic Ice Sheet. We map the perimeter and depth of a 260 km^2 surface depression above an Antarctic subglacial lake (SGL) and, in combination with Ice, Cloud and land Elevation Satellite laser altimetry, chart decadal changes in SGL volume. During 2007–2008, between 4.9 and 6.4 km^3 of water drained from the SGL, and peak discharge exceeded 160 $m^3 s^{-1}$. The flood was twice as large as any previously recorded and equivalent to ~10% of the meltwater generated annually beneath the ice sheet. The ice surface has since uplifted at a rate of 5.6 ± 2.8 m yr^{-1}. Our study demonstrates the ability of CryoSat-2 to provide detailed maps of ice sheet topography, its potential to accurately measure SGL drainage events, and the contribution it can make to understanding water flow beneath Antarctica.
Citation: McMillan, M., H. Corr, A. Shepherd, A. Ridout, S. Laxon, and R. Cullen (2013), Three-dimensional mapping by CryoSat-2 of subglacial lake volume changes, *Geophys. Res. Lett.*, *40*, doi:10.1002/grl.50689.

1. Introduction

[2] Satellite observations have provided evidence of a dynamic hydrological system beneath the Antarctic Ice Sheet (AIS) [*Gray et al*., 2005; *Wingham et al*., 2006a; *Fricker et al*., 2007; *Smith et al*., 2009]. The episodic outburst of water from lakes at the ice sheet base is a striking element of this system, with a capacity to trigger changes in ice flow [*Stearns et al*., 2008], floods into the oceans [*Fricker et al*., 2007], the rapid evolution of glacial landforms [*Lewis et al*., 2006], and disturbances to subglacial habitats. Active subglacial lakes were first identified using satellite radar altimetry and interferometry data, by interpreting isolated regions of vertical surface motion as evidence of water transfer at the ice sheet base [*Gray et al*., 2005; *Wingham et al*., 2006a]. Subsequent studies revealed that networks of active subglacial lakes were widespread [*Fricker et al*., 2007, 2010; *Fricker and Scambos*, 2009; *Smith et al*., 2009] and, together with modeling studies [*Pattyn*, 2008], suggested that lake drainage is a common feature of the subglacial system.

[1]School of Earth and Environment, University of Leeds, Leeds, UK.
[2]British Antarctic Survey, Cambridge, UK.
[3]Department of Earth Sciences, University College London, London, UK.
[4]European Space Agency, Noordwijk, Netherlands.

Corresponding author: M. McMillan, School of Earth and Environment, University of Leeds, Leeds LS2 9JT, UK. (m.mcmillan@leeds.ac.uk)

0094-8276/13/10.1002/grl.50689

[3] To date, 379 subglacial lakes have been identified beneath the AIS [*Wright and Siegert*, 2012]. Observations from the Ice, Cloud and land Elevation Satellite (ICESat) laser altimeter showed that approximately one third of lakes were active during a 5 year period [*Smith et al*., 2009]. These lakes have the capacity to store, and periodically release, some of the estimated 65 Gt of water generated annually through subglacial melting [*Pattyn*, 2010]. Determining the distribution, periodicity, and volume flux of lake drainage and refilling can benefit (1) models of subglacial hydrology [*Carter et al*., 2011], (2) estimates of subglacial melt rates and geothermal heat flux [*Pattyn*, 2010], (3) models of ice sheet flow, and (4) our understanding of freshwater delivery to subice shelf cavities [*Carter and Fricker*, 2012]. On a regional scale, accurate observations of lake volume fluctuations can help to characterize the short-term (~ decadal) variability superimposed upon secular ice mass trends.

[4] The current satellite record is limited in its ability to monitor lake volume fluctuations due to its sparse sampling in space or time, or because it is too short to capture full lake cycles. While repeat altimetry has provided regular observations, it is restricted by the increasing separation of ground tracks away from the pole and the coarse resolution of radar altimeters. As satellite tracks diverge away from the pole, constraining the area undergoing deformation is difficult, and volume change estimates are uncertain [e.g., *Fricker et al*., 2010]. In contrast, interferometric synthetic aperture radar can offer a detailed picture of the ice surface but is limited by the short, and often infrequent, acquisition periods. Furthermore, the recent termination of several satellite missions has severely limited current capacity to monitor lake evolution. Against this backdrop, the launch of the CryoSat-2 satellite [*Wingham et al*., 2006b] provides a new platform for monitoring active subglacial lakes. Here, we analyze observations from above an active subglacial lake, which were acquired by the CryoSat-2 altimeter operating in its novel interferometric mode. In combination with the complete 2003–2009 ICESat record, we detail the full spatial and temporal extent of a large subglacial outburst flood.

2. The $Cook_{E2}$ Subglacial Lake

[5] In this study we focus upon the $Cook_{E2}$ subglacial lake in East Antarctica, which was identified and named in the inventory published by *Smith et al*. [2009]. This active lake is situated at ~155.8°E, 72.8°S, close to the ice divide and beneath ~2700 m of slow-moving ice. Between November 2006 and March 2008, the ice surface fell by ~45 m, about five times the magnitude of any other observed lake signal. During this period, the lake was estimated to have lost 2.7 km^3 of water, although volume loss was poorly

Table 1. Parameters Used to Estimate CryoSat-2 Resolution

	Description	Value
W	Hamming widening factor	1.30
R_e	Earth's radius	6,378,137 m
λ	Carrier wavelength	0.0221 m
z_{sat}	Satellite altitude	710,000–755,000 m
PRF	Pulse repetition frequency	18.2 kHz
N	Number of pulses per closed burst used to form synthetic aperture	64
v_{sat}	Satellite velocity	7,500 ms^{-1}
B	Measured bandwidth	320 MHz

constrained by only two ICESat reference tracks passing over the lake [*Smith et al*., 2009].

3. CryoSat-2 Data

[6] CryoSat-2 was launched in April 2010 and operates the first Earth-observing satellite altimeter with interferometric capability [*Wingham et al*., 2006b]. We used data acquired during January–November 2011, with the altimeter operating in synthetic aperture radar interferometric (SARin) mode. In this mode, CryoSat-2 transmits bursts of pulses at a high pulse repetition frequency, which enables the along-track ground resolution to be improved through coherent processing of the radar echoes. Additionally, within the ~15 km beam-limited footprint, the across-track angle of arrival of echoes can be determined from the phase difference measured across the two onboard antennas.

[7] The algorithms used to process the CryoSat-2 data largely follow those described by *Wingham et al*. [2006b], with two notable exceptions. First, the raw echoes have been oversampled by a factor of 2 in order to remove aliasing over specular surfaces. As a result, the range window has been halved (240 to 120 m) to maintain a consistent product size. Second, a Hamming weighting function has been applied to suppress the side lobes of the synthetic beams. This weighting has the effect of widening the main beam and reducing along-track resolution. Using the operating parameters described in Table 1, the resulting along-track resolution can be estimated as follows:

$$\delta x \approx 0.886\ W\ z_{sat} \left(1 + \frac{z_{sat}}{R_e}\right) \left(\frac{\lambda\ PRF}{2\ N\ v_{sat}}\right). \quad (1)$$

[8] This expression formulates the half power angular beam width from the instrument sampling along the synthetic aperture and projects the Hamming-weighted beam onto a curved Earth surface. The resulting along-track resolution falls in the range of 380–410 m, depending upon satellite altitude, and is larger than the ~300 m along-track instrument sampling. In the across-track plane, the pulse-limited resolution at the point of closest approach to the satellite, or more generally at any point where the local incidence angle at the surface is zero, is given by

$$\delta y \approx 2 \left(1 + \frac{z_{sat}}{R_e}\right) \sqrt{0.886\ z_{sat}\ c\ \frac{1}{B}}. \quad (2)$$

[9] For CryoSat-2 operating parameters (Table 1), the across-track resolution is ~1.7 km (prior to oversampling).

[10] To assess the accuracy of SARin observations, we firstly considered errors in the measurement of the range and the angle of arrival of the echo and secondly evaluated the product against independent data. Several sources of range error have been identified to date, namely (1) a datation error which may contribute < 2 cm to the range measurement and (2) a −0.67 m bias due to the mishandling of internal instrument path delays (−0.77 m) and the offset between the satellite center of mass and antenna reference point (+0.10 m). In the context of this study, the datation error is negligible and the bias is addressed in more detail below. Turning to the accuracy of the angle-of-arrival measurements, spatially varying errors of several hundred microradians are caused by (1) bending of the antenna bench, which affects the estimate of baseline orientation, and (2) a slope dependency within the interferometric measurements [*Galin et al*., 2013; *Gray et al*., 2012]. Although these errors have a small (~ 5 cm) impact upon elevation measurements, they may introduce an error of several hundred meters into the across-track ground positioning of the echo. These errors remain small relative to the spatial scale of the topographic feature mapped in this study.

[11] We evaluated CryoSat-2 measurements using ICESat altimetry from 2003 to 2009 (GLA06 product, Release 633 [*Zwally et al*., 2003]) over a ~7.5×10^3 km^2 area which surrounded the $Cook_{E2}$ lake site and which we assumed was largely stable during the 2003–2011 observation period. We compared each ICESat measurement to a colocated elevation estimate formed from a bilinear interpolation of the surrounding CryoSat-2 data. We applied the sensor saturation range correction supplied with the ICESat product and removed measurements where it was lacking (records with zero saturation correction were not discarded). To maximize data coverage, no records were removed based upon evidence of atmospheric forward scattering of the laser signal. This may introduce decimeter-level elevation biases to our measurements [*Duda et al*., 2001; *Siegfried et al*., 2011], but these remain 2 orders of magnitude less than the signal we observe. There was generally good agreement between the two data sets (Figure 1). Examining the intersatellite elevation differences, we find a bias of −1.5 m (CryoSat-2 minus ICESat) and a standard deviation of 0.9 m. After accounting for the −0.67 m CryoSat-2 instrument bias, we attribute the remaining −0.83 m offset to the effect of radar penetration into the snowpack, which has been seen by airborne observations at Ku band frequencies [*Hawley et al*., 2006]. We subtract the total (−1.5 m) bias from all CryoSat-2 elevation measurements to prevent it from contributing to elevation change estimates.

[12] Turning now to the 0.9 m intersatellite standard deviation, in addition to any altimeter range imprecision, for example arising from the retracking of the echo, several factors may contribute to this value. First, CryoSat-2 data were interpolated to ICESat shot locations, and so any small-scale topography not resolved by our interpolation will introduce elevation differences. This may explain some of the spatially correlated outliers that appear as curves in Figure 1. Second, ICESat and CryoSat-2 data were collected during different years, and so accumulation fluctuations may manifest as elevation differences. Third, ICESat has a much smaller footprint than CryoSat-2, and therefore, we are

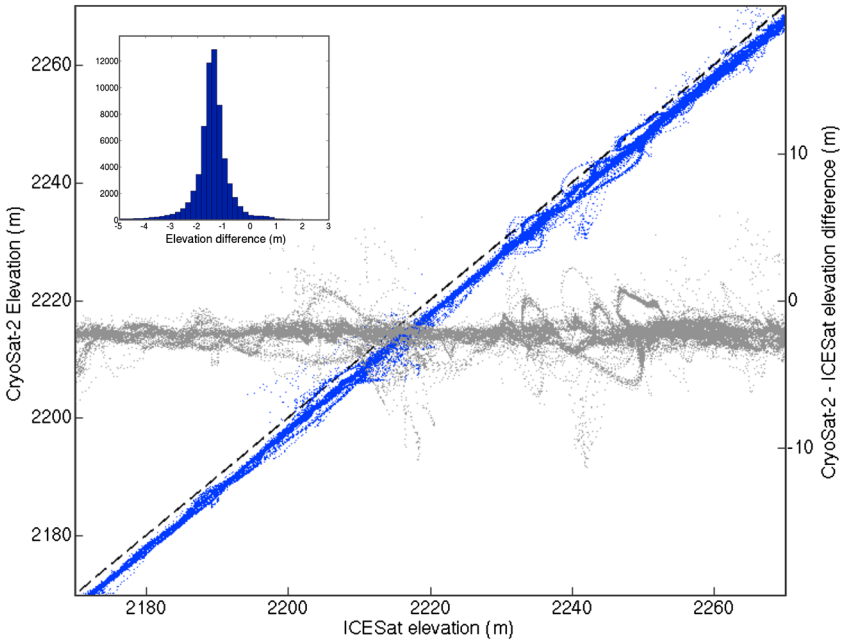

Figure 1. Comparison of ICESat and CryoSat-2 elevations from a ~ 7.5×10^3 km^2 area surrounding the Cook$_{E2}$ subglacial lake. The elevation comparison is shown in blue (black dashed line indicates equivalence), and the difference between each CryoSat-2 and ICESat elevation measurement is in grey. The comparison was performed by evaluating an interpolation of the CryoSat-2 data along ICESat tracks. The inset shows the distribution of CryoSat-2 minus ICESat elevation differences.

comparing observations made over different spatial scales. Finally, some ICESat records may include an additional range delay due to atmospheric forward scattering.

4. Ice Surface Topography from CryoSat-2

[13] To map ice surface topography above the Cook$_{E2}$ subglacial lake, we formed a minimum curvature interpolation [*Sandwell*, 1987] of the CryoSat-2 data and posted elevations on a 100 m grid (Figure 2). CryoSat-2 maps the ice surface with remarkable detail, a result of both the SARin processing and the closely spaced ground tracks. Previously, ICESat data from two intersecting tracks had indicated a deep hollow [*Smith et al*., 2009], but the shape of this feature had, until now, remained unclear. Of particular note is the ability of the interferometer to track the perimeter of the surface hollow (Figure 2a). This novel capability, combined with the echoes received from deep within the depression, allows the area and depth of this feature to be mapped by a single altimeter instrument. We estimate the area of the depression to be 260 km^2 by differencing predrainage and postdrainage surface elevation models (formed from interpolations of ICESat data from 2003 and CryoSat-2 data from 2011, respectively). The depression domain was defined as all grid cells where the 2003–2011 elevation change exceeded the 3σ intersatellite elevation variability, as calculated along ICESat tracks surrounding the lake. The comprehensive coverage provided by CryoSat-2 enables the full spatial extent of this feature to be mapped with confidence, with ~ 80% of the depression perimeter being within 500 m of a CryoSat-2 measurement.

[14] The SARin mode echoes provide additional information on how the instrument resolves the ice surface. We picked two consecutive SARin echoes, where the altimeter switched from tracking the rim to tracking the interior of the depression. Examining received power and coherence across the full range window (Figures 2c and 2d) indicates that the echoes are broadly similar in shape. In both cases, there are multiple coincident peaks in power and coherence, suggesting a coherent signal from a number of distinct locations within the beam footprint. This observation is encouraging because it suggests that there is useful geophysical information beyond the point of closest approach. More specifically, the two largest peaks within the range window correspond to backscatter from the rim and the interior of the depression (Figures 2c and 2d). The strong returns suggest in both cases a relatively large pulse-limited footprint and that at both locations the incidence angle at the surface is close to zero. In the two echoes studied here, the retracker switches between the two peaks because it is designed to track the strongest power return. However, this analysis demonstrates the potential to track multiple features in both echoes and, more generally, to implement full swath processing in areas with suitable surface gradients [*Hawley et al*., 2009; *Gray et al*., 2012].

5. Ice Surface Elevation Change

[15] We used the CryoSat-2 and ICESat data to investigate the 2003–2011 surface elevation changes above the Cook$_{E2}$ lake (Figure 3) by extracting an elevation time series from the deepest part of the depression crossed by repeated ICESat tracks (location shown in Figure 4e). Because ICESat reference tracks are repeated with an across-track precision of ~ 110 m [*Siegfried et al*., 2011], successive campaigns must be corrected for surface slope. Here, because the elevation change is unusually large, we varied our slope correction in time as the depression formed. For each ICESat campaign, we combined the ICESat data with the CryoSat-2 observations from 2011 to form a time series of

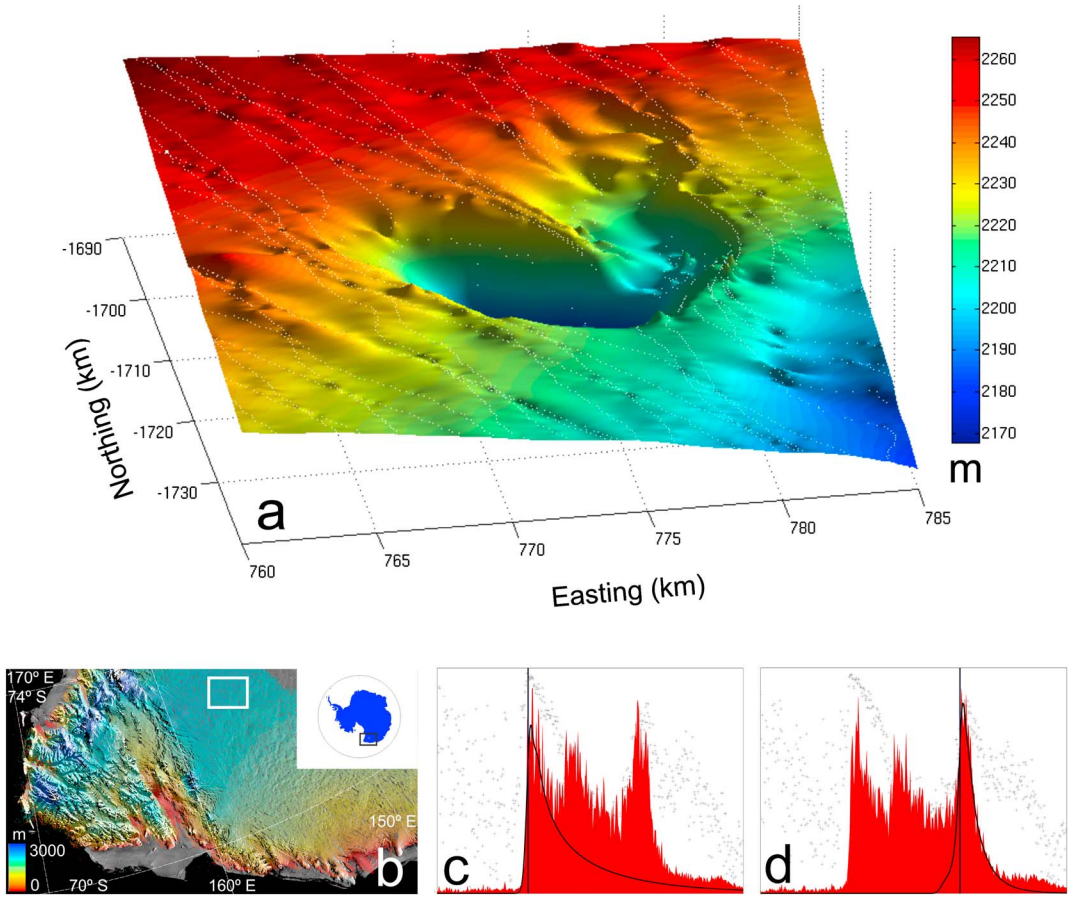

Figure 2. (a) Surface expression of the drained $Cook_{E2}$ subglacial lake, mapped by CryoSat-2 interferometric mode data (white dots) acquired between January and November 2011. The colored surface depicts a minimum curvature interpolation of the CryoSat-2 data and is presented as a shaded relief illuminated from the east. (b) Location of the $Cook_{E2}$ subglacial lake. Colored tracks are CryoSat-2 SARin elevation measurements, and background image is from the Moderate Resolution Imaging Spectroradiometer mosaic of Antarctica [*Haran et al.*, 2005]. (c, d) Power (red) and coherence (black dots) of two consecutive SARin mode echoes, where the altimeter switched from tracking the rim (Figure 2c) to the bottom (Figure 2d) of the surface depression. The black curve shows the retracker fit to the echo power, and the vertical black line marks the retracking point used to determine elevation.

elevation models. In detail, we compared the ICESat data that crossed the surface depression with the coincident CryoSat-2 elevations from our surface map (Figure 2). We estimated (1) the strength of the linear correlation and (2) a linear model that related the two data sets. When a strong correlation existed (2007–2009 inclusive, $R^2 > 0.95$), we assumed that an elevation model based on the CryoSat-2 observations could adequately characterize the topography of the depression. In practice, this holds whenever one depth profile can be scaled and shifted in the vertical axis so as to closely match the second profile. We then used the linear model to transform the CryoSat-2 elevations into an estimate of surface elevation at the time of the ICESat campaign. By definition, this achieved a least squares best fit to the sparse ICESat data and was used to correct for surface slope. When ICESat and CryoSat-2 data were not correlated (prior to 2007), we used a reference surface formed from the 2003 ICESat data for the same purpose.

[16] The elevation time series (Figure 3) shows three distinct phases of surface evolution: first, stable elevations, followed by rapid subsidence and then finally surface uplift. To provide a simple characterization of this behavior, we fitted a linear trend to each of these three phases. Between 2004 and 2006, the ice surface at this location was stable ($0.0 \pm 0.2\,m\,yr^{-1}$ elevation trend). Thereafter, the ice surface began to subside, falling a total of ~70 m by the end of 2008, at an average rate of $35 \pm 14\,m\,yr^{-1}$. The uncertainty, which is represented by the 95% confidence interval (CI) of the fitted trend, results in part from our approximation that the surface subsides at a constant rate and also from the poorly constrained endpoints of the drainage event. Errors in the data themselves, such as slope correction errors or ICESat intercampaign biases, only make a small contribution to the trend uncertainty because (1) the magnitude of our slope correction at this location is at most 0.45 m and (2) intercampaign biases in ICESat observations are less than ~0.2 m [*Siegfried et al.*, 2011]. Following the termination of surface subsidence, the ice surface began to rise at a rate of $5.6 \pm 2.8\,m\,yr^{-1}$ (95% CI). Assuming no acceleration in the uplift rate, it will take at least another 8 years for the ice surface to reach the level where the lake drained previously.

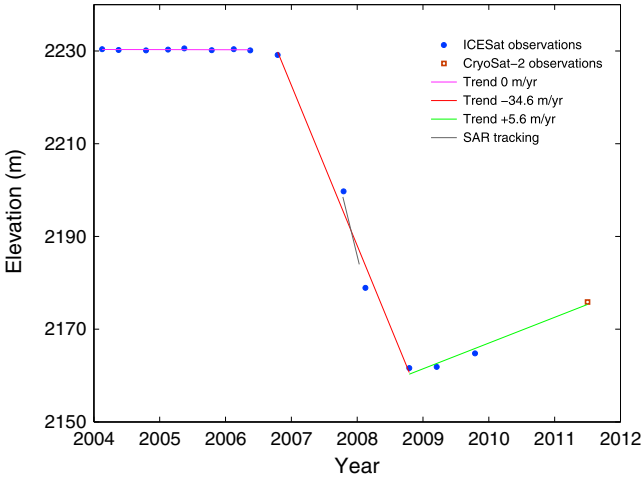

Figure 3. Evolution of ice surface elevation above the $Cook_{E2}$ subglacial lake, from ICESat (2003–2009) and CryoSat-2 (2011) observations. An independent estimate of elevation change derived from SAR feature tracking is also shown and has been referenced to the modeled elevation trend (red line) for comparison. The location of the time series is shown in Figure 4e.

6. Lake Volume Evolution

[17] We estimated the volume of water discharged during the $Cook_{E2}$ outburst flood from surface elevation changes, under the assumption that surface depression and lake volume changes were equivalent [*Fricker et al.*, 2007; *Smith et al.*, 2009]. We did not estimate the volume rate of lake refilling because surface uplift may in part have been driven by the flow of ice into the newly created hollow. Surface elevation maps were estimated annually and converted to depth grids by subtracting a reference surface (formed from all ICESat data collected in 2003). Finally, the volume of the surface depression was estimated by integrating depths over the lake domain. The sparse ICESat data clearly resolve the depth evolution along the ICESat tracks; however, the full area extent, and hence volume, is poorly constrained (Figure 4). In particular, following the initiation of ICESat's campaign mode in 2004, ICESat tracks do not cross the shallower part of the depression situated to the north east of the main depression (hereafter termed the NE lobe). As a result, we cannot be certain that the NE lobe evolved in a similar manner to the main depression during the drainage event. To account for this uncertainty, we explore two possible scenarios which provide bounds on the volume of the lake drainage event.

[18] First, we assume that the NE lobe did not form simultaneously with the main depression. This allows for the possibility that the uplift observed within the main depression from ~2009 onwards (Figure 3) was driven by a transfer of water from the NE lobe or by a local acceleration in ice flow in response to the main drainage event. In this case, we estimate the magnitude of the subglacial outburst flood to be 4.85 km^3, calculated simply as the volume of the surface depression resolved by CryoSat-2 in 2011 (Figure 4e). This represents a conservative measure of the

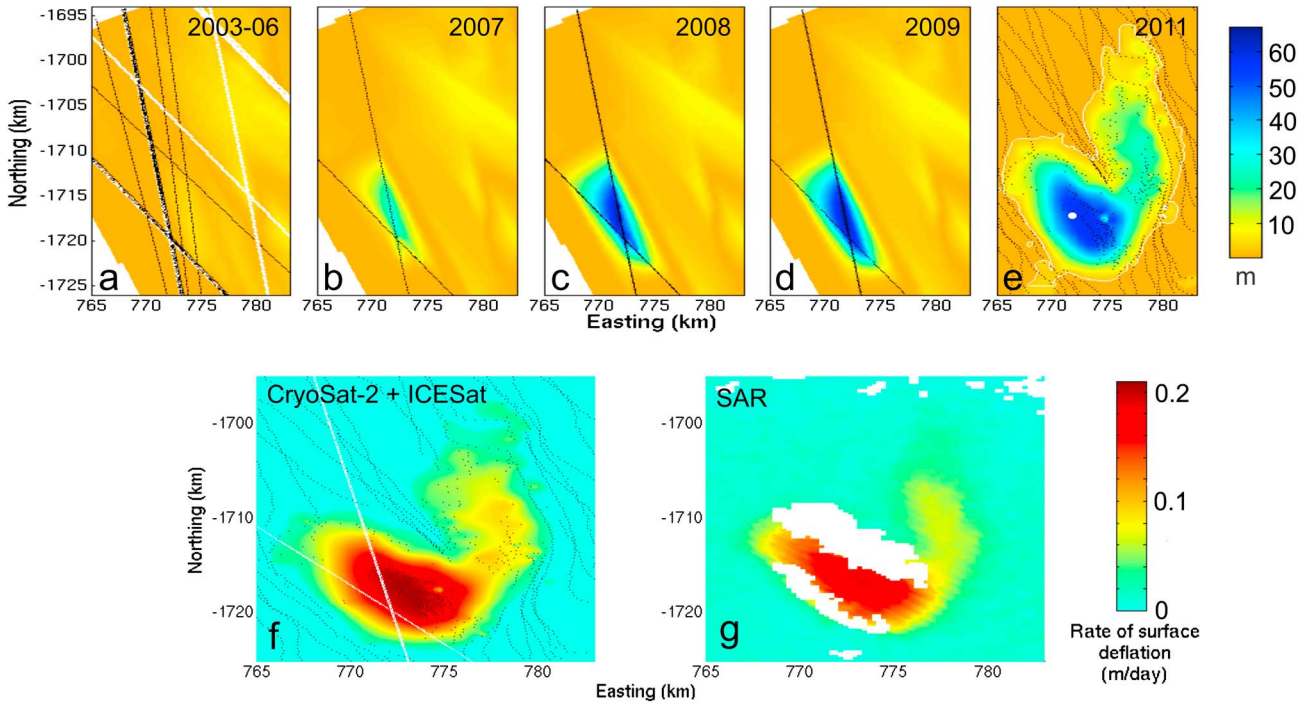

Figure 4. The depth evolution and rate of subsidence of the ice surface depression above the $Cook_{E2}$ subglacial lake. The images at the top show the evolution in depth as observed by (a–d) ICESat and (e) CryoSat-2. The black tracks locate data acquisitions, the white tracks in Figure 4a are those made by ICESat in 2003, the white line in Figure 4e identifies the depression boundary, and the white circle in Figure 4e marks the time series shown in Figure 3. The images at the bottom show a comparison of the rate of subsidence (f) from the combined ICESat (white tracks) and CryoSat-2 (black tracks) observations and (g) from a pair of ALOS SAR images acquired on 12 October 2007 and 12 January 2008. The white areas in Figure 4g are regions where no coherent displacement signal was retrieved.

2007–2008 outburst flood since we estimate only the net volume lost between 2003 and 2011, a period which likely also included lake refilling. If all water were discharged over the period of surface lowering identified in Figure 3, then lake drainage occurred at a mean rate of $97\,m^3\,s^{-1}$.

[19] Second, we assume that both the main depression and the NE lobe evolved simultaneously and that the behavior observed along ICESat tracks (for example, Figure 3) is representative of the whole depression. We then derive an upper bound on volume discharge by using a simple model to extrapolate the elevation changes observed along ICESat tracks over the entire depression resolved by CryoSat-2. We follow the method used for our slope correction, whereby we use the interpolated CryoSat-2 data as a template for the shape of the depression and model this feature in earlier years by scaling this surface so that it best fits, in a least squares sense, the ICESat data from each campaign. This effectively stretches or compresses the CryoSat-2 surface in the vertical axis so as to fit the ICESat observations while forcing depths to tend to zero at the perimeter of the 2011 depression. This approach yields an upper bound of $6.36\,km^3$ on the water drained during the outburst flood and a peak discharge in excess of $160\,m^3\,s^{-1}$. As a result of resolving the full spatial and temporal extent of this event, our estimate of water drained is ~2.5 times greater than that determined previously [*Smith et al*., 2009] and represents the largest subglacial lake outburst flood inferred from satellite data to date.

7. Independent Evaluation

[20] To assess our upper bound volume estimate, and the model upon which it is based, we compared the deflation rate predicted by the model to an independent estimate derived from a pair of Advanced Land Observing Satellite (ALOS) SAR images (Figures 4f and 4g). These data were acquired on 12 October 2007 and 12 January 2008 and provide a 92 day snapshot of ice displacement at the peak of the flood. We used GAMMA software (http://www.gamma-rs.ch) to estimate surface elevation change using a backscatter intensity feature-tracking algorithm. Displacement in the radar line of sight was estimated by matching image patches with dimensions of $\sim 950 \times 850$ m in ground coordinates. The azimuth component of displacement was neglected due to its insensitivity to vertical motion. Because both horizontal and vertical ice motion are resolved as displacement in the radar line of sight, we measured displacement relative to the background signal. This removed any contribution from uniform ice flow across the SAR image. We interpreted all remaining signal as vertical motion. At the location of our elevation time series (Figure 3), the ALOS-derived rate of surface subsidence is in excellent agreement with the rate determined using our model ($0.16\,m\,day^{-1}$ from ALOS; $0.17\,m\,day^{-1}$ from our model). Together with the strong similarity in the spatial pattern of deformation predicted by both approaches (Figures 4f and 4g), this evaluation supports the upper bound estimate we make.

8. Summary

[21] We have mapped the ice surface above a drained subglacial lake using CryoSat-2 interferometric altimetry. This study demonstrates the capability of CryoSat-2 to deliver high-resolution surface elevation measurements and the novel ability of the instrument to track topographic features. Our observations show that a single subglacial lake discharged ~6 Gt of water during a period of ~20 months. To provide context, this is equivalent to ~10% of annual subglacial melting beneath the AIS [*Pattyn*, 2010] or alternatively, ~8% of the yearly AIS mass imbalance [*Shepherd et al*., 2012]. Our observations provide evidence that a significant fraction of the AIS subglacial meltwater budget can be moved in discrete, episodic events. Continued surveys are required to ascertain the frequency of large drainage events, in order to determine whether this represents the dominant mode of water transport. Such information is valuable not only for developing realistic hydrological models [*Carter et al*., 2011], but also for understanding the impact upon ice dynamics of variable rates of water delivery into the subglacial system [e.g., *Bartholomew et al*., 2012]. Finally, these observations show that lake drainage can cause fluctuations in mass and surface elevation over subdecadal timescales. This reinforces the need to estimate ice sheet mass balance over timescales longer than the periodicity of lake evolution and suggests that some of the short-term variability in mass balance estimates [*Shepherd et al*., 2012] may be attributable to subglacial water transfer.

[22] **Acknowledgments.** This work was supported by the UK Centre for Polar Observation and Modelling. ICESat data were provided by the National Snow and Ice Data Centre, and ALOS data by the European Space Agency. We are grateful to N. Galin and M. Fornari for discussions relating to CryoSat-2 performance, and thank H. A. Fricker, T. Flament and several anonymous reviewers for comments which substantially improved this paper.

[23] The Editor thanks Helen Fricker and an anonymous reviewer for their assistance in evaluating this paper.

References

Bartholomew, I., P. Nienow, A. Sole, D. Mair, T. Cowton, and M. A. King (2012), Short-term variability in Greenland Ice Sheet motion forced by time-varying melt-water drainage: Implications for the relationship between subglacial drainage system behavior and ice velocity, *J. Geophys. Res.*, *117*, F03002, doi:10.1029/2011JF002220.

Carter, S. P., and H. A. Fricker (2012), The supply of subglacial meltwater to the grounding line of the Siple Coast, West Antarctica, *Ann. Glaciol.*, *53*(60), 267–280.

Carter, S. P., H. A. Fricker, D. D. Blankenship, J. V. Johnson, W. H. Lipscomb, S. F. Price, and D. A. Young (2011), Modeling 5 years of subglacial lake activity in the MacAyeal Ice Stream (Antarctica) catchment through assimilation of ICESat laser altimetry, *J. Glaciol.*, *57*(206), 1098–1112.

Duda, D., J. Spinhirne, and E. Eloranta (2001), Atmospheric multiple scattering effects on GLAS altimetry - Part I: Calculations of single pulse bias, *IEEE Trans. Geosci. Remote Sens.*, *39*(1), 92–101, doi:10.1109/36.898668.

Fricker, H. A., and T. Scambos (2009), Connected subglacial lake activity on lower Mercer and Whillans Ice Streams, West Antarctica, 2003–2008, *J. Glaciol.*, *55*(190), 303–315.

Fricker, H. A., T. Scambos, R. Bindschadler, and L. Padman (2007), An active subglacial water system in West Antarctica mapped from space, *Science*, *315*(5818), 1544–1548, doi:10.1126/science.1136897.

Fricker, H. A., T. Scambos, S. Carter, C. Davis, T. Haran, and I. Joughin (2010), Synthesizing multiple remote-sensing techniques for subglacial hydrologic mapping: Application to a lake system beneath MacAyeal Ice Stream, West Antarctica, *J. Glaciol.*, *56*(196), 187–199.

Galin, N., D. Wingham, R. Cullen, M. Fornari, W. H. F. Smith, and S. Abdalla (2013), Calibration of the CryoSat-2 interferometer and measurement of across-track ocean slope, *Geosci. Remote Sens.*, *51*(1), 57–72, doi:10.1109/TGRS.2012.2200298.

Gray, L., I. Joughin, S. Tulaczyk, V. Spikes, R. Bindschadler, and K. Jezek (2005), Evidence for subglacial water transport in the West Antarctic Ice Sheet through three-dimensional satellite radar interferometry, *Geophys. Res. Lett.*, *32*, L03501, doi:10.1029/2004GL021387.

Gray L., D. Burgess, L. Copland, N. Galin, and R. Cullen (2012), Using the CryoSat interferometric swath mode for glacial ice topography, Proceedings of the Earth Observation and Cryosphere Science Conference, ESA Special Publications 712.

Haran, T., J. Bohlander, T. Scambos, T. Painter, and M. Fahnestock (2005), MODIS mosaic of Antarctica (MOA) image map, National Snow and Ice Data Centre, Boulder, Colorado.

Hawley, R. L., E. M. Morris, R. Cullen, U. Nixdorf, A. P. Shepherd, and D. J. Wingham (2006), ASIRAS airborne radar resolves internal annual layers in the dry-snow zone of Greenland, *Geophys. Res. Lett.*, *33*, L04502, doi:10.1029/2005GL025147.

Hawley, R. L., A. Shepherd, R. Cullen, and D. J. Wingham (2009), Ice-sheet elevations from across-track processing of airborne interferometric radar altimetry, *Geophys. Res. Lett.*, *36*, L25501, doi:10.1029/2009GL040416.

Lewis, A., D. Marchant, D. Kowalewski, S. Baldwin, and L. Webb (2006), The age and origin of the Labyrinth, western Dry Valleys, Antarctica: Evidence for extensive middle Miocene subglacial floods and freshwater discharge to the Southern Ocean, *Geology*, *34*(7), 513–516, doi:10.1130/G22145.1.

Pattyn, F. (2008), Investigating the stability of subglacial lakes with a full Stokes ice-sheet model, *J. Glaciol.*, *54*(185), 353–361, doi:10.3189/002214308784886171.

Pattyn, F. (2010), Antarctic subglacial conditions inferred from a hybrid ice sheet/ice stream model, *Earth Planet. Sci. Lett.*, *295*(3–4), 451–461, doi:10.1016/j.epsl.2010.04.025.

Sandwell, D. (1987), Biharmonic spline interpolation of GEOS-3 and Seasat altimeter data, *Geophys. Res. Lett.*, *14*(2), 139–142.

Shepherd, A., et al. (2012), A reconciled estimate of ice-sheet mass balance, *Science*, *338*(6111), 1183–1189, doi:10.1126/science.1228102.

Siegfried, M., R. Hawley, and J. Burkhart (2011), High-resolution ground-based GPS measurements show intercampaign bias in ICESat elevation data near Summit, Greenland, *IEEE Trans. Geosci. Remote Sens.*, *49*(9), 3393–3400, doi:10.1109/TGRS.2011.2127483.

Smith, B., H. A. Fricker, I. Joughin, and S. Tulaczyk (2009), An inventory of active subglacial lakes in Antarctica detected by ICESat (2003–2008), *J. Glaciol.*, *55*(192), 573–595.

Stearns, L., B. Smith, and G. Hamilton (2008), Increased flow speed on a large East Antarctic outlet glacier caused by subglacial floods, *Nat. Geosci.*, *1*(12), 827–831, doi:10.1038/ngeo356.

Wingham, D. J., M. J. Siegert, A. Shepherd, and A. S. Muir (2006a), Rapid discharge connects Antarctic subglacial lakes, *Nature*, *440*(7087), 1033–1036, doi:10.1038/nature04660.

Wingham, D. J., et al. (2006b), CryoSat: A mission to determine the fluctuations in Earth's land and marine ice fields, *Adv. Space Res.*, *37*, 841–871, doi:10.1016/j.asr.2005.07.027.

Wright, A., and M. Siegert (2012), A fourth inventory of Antarctic subglacial lakes Antarctic, *Science*, *24*(06), 659–664, doi:10.1017/S095410201200048X.

Zwally, H., R. Schutz, C. Bentley, J. Bufton, T. Herring, J. Minster, J. Spinhirne, and R. Thomas (2003), GLAS/ICESat L2 Antarctic and Greenland Ice Sheet Altimetry Data V018. Boulder, CO: National Snow and Ice Data Center. Digital media.